nism, but double stars measured before and after the Io observations showed no obvious difference. We suspect that the cause is the existence of other, weaker hot spots on the disk. For example, a hot spot near the western limb (230° to 250°) would increase the apparent east-west diameter, would shift the center of the modeled disk relative to the hot spot, and would increase the disk's relative brightness. The greater scatter in the east-west diameter, compared with that in the north-south, also suggests such an effect. However, because this is a new technique with perhaps unknown sources of error, we do not claim that the presence of such a hot spot is firmly required by the residuals.

Finally, the systematic effects mentioned above, which introduce spurious high-frequency power, resulted in an overestimate of the hot spot brightness. This spurious power adds in quadrature with the true power. Estimating that it would result in a visibility of 0.15 for a completely resolved disk, and subtracting the equivalent power, we obtained a corrected hot spot brightness of 0.67 when it is at the subearth point.

Measurements of the total brightness of Io, relative to the star λ Sgr, allowed us to estimate the hot spot flux. Adopting an M magnitude of 0.438 ± 0.005 for this star (*5*) and a zero magnitude flux of 170 ± 8 Jy (*7*), we obtained a hot spot flux of 5.78 Jy, which is equivalent to a radiance at Io's surface of 2.96×10^{22} ergs sec^{-1} cm^{-1} sr^{-1}/A, where A is the hot spot area.

In summary, after correcting for systematic effects and estimating the various sources of error, we adopt the following hot spot parameters: longitude, 301° ± 6°; latitude, 10° ± 6°; brightness, 0.67 ± 0.15 (relative to the disk); radiance, $(2.96 \pm 0.54) \times 10^{22}$ ergs sec^{-1} cm^{-1} sr^{-1}/A.

These data, when combined with the knowledge that an infrared outburst was occurring (*5*), indicate that an eruption was taking place in the Loki region. Loki Patera, the "lava lake" seen by Voyager, was located at (309°, +12°) (*8*). Two plumes issued from opposite ends of a dark feature slightly to the northeast: (305°, +19°) and (301°, +17°) (*9*). All these locations are slightly beyond the errors limits we have quoted for our measurements. The discrepancy is small enough that we cannot absolutely exclude them, but the polarization observations by Goguen and Sinton (*5*) also suggest a source slightly east of Loki Patera. (In this case, east is the direction on the planet, not on the plane of the sky.)

Table 1. North-south hot spot position on 3 July 1984.

Universal time (hours)	Location (arc seconds)	Longitude (degrees)
10:52	0.125	+13
10:58	0.176	18
11:08	0.044	5
11:13	0.007	2
11:21	0.122	13

We can derive an area for the hot spot from the radiance, but the result is highly dependent on the temperature assumed. For example, 400 K corresponds to 11,400 km^2, 600 K to 930 km^2, and 800 K to 260 km^2. For comparison, the overall area of Loki Patera was 50,000 km^2. In view of the large area required for any likely temperature, the source must be similar to a lava lake or flow rather than to the small vent of a plume. The position of the active part of the lava lake may have shifted. Voyager images (*10*) show evidence for several such shifts in the past, in the form of partly "solidified" or obscured sections extending to the northeast and southwest.

The recent development of techniques that allow observations of individual hot spots, such as the speckle observations described here, together with the work of Goguen and Sinton (*5*), should contribute toward a much improved understanding of volcanism on Io. Multiple wavelength observations will be particularly important because they will allow accurate estimates to be made of the hot spot temperatures and thus of the relative importance of silicate and sulfur volcanism.

References and Notes

1. T. V. Johnson *et al.*, *Science* **226**, 134 (1984).
2. H. M. Dyck and R. R. Howell, *Astron. J.* **87**, 400 (1982).
3. K. T. Knox and B. J. Thompson, *Astrophys. J.* **193**, L45 (1974).
4. J. R. Fienup and G. B. Feldkamp, *Proc. Soc. Photo-Opt. Instrum. Eng.* **243**, 95 (1980); J. G. Walker, *Appl. Opt.* **21**, 3132 (1982); J. C. Dainty, *Top. Appl. Phys.* **9**, 255 (1984).
5. J. D. Goguen and W. M. Sinton, *Science* **230**, 65 (1985).
6. One highly discrepant observation was obtained at 9:33 UT, indicating a disk diameter of 0.511 arc second, a brightness of 1.933, and a position of 0.467 arc second. This diameter is less than half the true value, the brightness is more than twice that of any other measurement, and the longitude is also inconsistent. We have deleted this point from the fits and the figures, but we do not understand the source of the error.
7. H. C. Campins *et al.*, *Astron. J.* **90**, 896 (1985). 1 Jansky = 10^{-26} W m^{-2} Hz^{-1}.
8. G. G. Schaber, in *Satellites of Jupiter*, D. M. Morrison, Ed. (Univ. of Arizona Press, Tucson, 1982), pp. 556–597; J. C. Pearl and W. M. Sinton, *ibid.*, pp. 724–755.
9. R. G. Strom and N. M. Schneider, *ibid.*, pp. 598–633.
10. The cover of the *Science* issue containing (*1*) is an excellent example.

11. We thank J. Goguen and W. Sinton for helpful discussions. This work was supported in part by NSF grant AST 82-08793 and NASA grant NASW3135. The Infrared Telescope Facility is operated by the University of Hawaii under contract from NASA.

1 April 1985; accepted 30 May 1985

Characterization of Io's Volcanic Activity by Infrared Polarimetry

Abstract. *The thermal emission from Io's volcanic hot spots is linearly polarized. Infrared measurements at 4.76 micrometers show disk-integrated polarization as large as 1.6 percent. The degree and position angle of linear polarization vary with Io's rotation in a manner characteristic of emission from a small number of hot spots. A model incorporating three hot spots best fits the data. The largest of these hot spots lies to the northeast of Loki Patera, as mapped from Voyager, and the other spot on the trailing hemisphere is near Ra Patera. The hot spot on the leading hemisphere corresponds to no named feature on the Voyager maps. The value determined for the index of refraction of the emitting surface is a lower bound; it is similar to that of terrestrial basalts and is somewhat less than that of sulfur.*

Jay D. Goguen
William M. Sinton
University of Hawaii, Institute for Astronomy, Honolulu 96822

Io is the only body in the solar system, other than Earth, on which active volcanism has been observed directly. During the two Voyager encounters (March and July 1979), nine plumes were detected on Io above active vents on a young, craterless volcanic terrain; these features are indicative of vigorous, sustained eruptive activity (*1, 2*). Ground-based infrared (IR) photometry of the thermal emission from Io's hot spots has shown a stable, long-wavelength (8 to 20 μm) component (*3*) and a variable, short-wavelength (5 μm) component (*4*). Ground-based IR measurements do not resolve the disk and represent hemispheric averages. Disk-integrated measurements of the linear polarization of the thermal emission as Io rotates is a new technique that can be used to locate hot spots in both latitude and longitude, to measure the flux emitted from individual hot spots, and to estimate the index

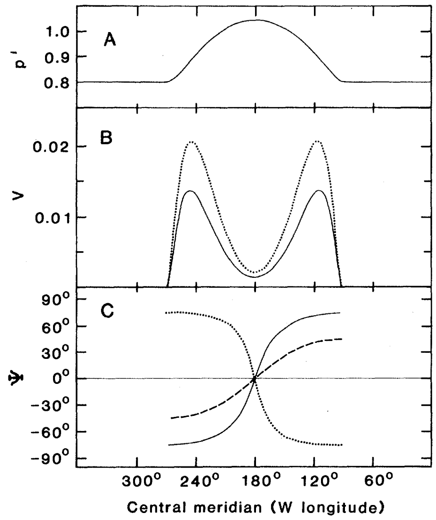

Fig. 1. The variation of flux and linear polarization with orbital longitude due to a single standard hot spot of area 2000 km^2 (T, 450 K) located at 180°W, 15°N on a model planet with n = 1.5 and a true geometric albedo of 0.8. In each frame of the figure, the solid line is the signature of this standard spot and the broken lines show the changes in this signature if one of the parameters is varied from the standard configuration. (A) The effective geometric albedo, p'. (B) The degree of linear polarization, V (dotted line, n = 1.8). (C) Position angle of linear polarization, ψ (dashed line, latitude 45°N; dotted line, latitude 15°S).

of refraction of the emitting surface. A series of rotational polarization curves can be used to establish the volcanic context of the Io data from the upcoming Galileo mission. Ground-based measurements made during Galileo's approach to Jupiter may provide timely targeting information on active eruption sites when the spacecraft has its only close encounter with Io immediately upon insertion into orbit around Jupiter.

Thermal radiation is initially unpolarized when it originates beneath the surface and becomes linearly polarized upon transmission across the surface boundary. The surface boundary is assumed to be a smooth interface between the dielectric surface material with real index of refraction n and a vacuum with n = 1.0. Kirchoff's law requires that the emissivity of the surface be the complement of the reflectivity for each polarization. The reflectivity is given by Fresnel's reflection coefficients (*5, 6*). The emitted radiation (viewed by an observer on the vacuum side of the interface) is linearly polarized, with its electric vector preferentially coplanar with the normal to the surface and the line of sight. The degree of polarization increases as the line of sight deviates from the surface normal (more grazing viewing); the degree of polarization increases with n.

Because the arc-second disk of Io is too small to be resolved by ground-based telescopes (*7*), a quantitative model must calculate the net polarization that results from integration of the emission and diffuse reflection of sunlight from many flat surface elements distributed over a sphere. At 5 μm, most of the background flux from Io is reflected sunlight (*3, 4*). Near opposition, linear polarization of this reflected flux is negligible (*8*). We have assumed that zero linear polarization is introduced by the background flux from areas that are not hot spots.

The assumption of zero background polarization means that the observed polarization can be interpreted as the sum of the contributions of hot spots. Consider the contribution of a single hot spot of area A at an angular distance θ from the center of Io's disk. A convenient unit is the product of the Planck function for the relevant temperature, $B(T)$, and the solid angle ω subtended by the spot, $\omega = A/d^2\cos\theta$, where d is the distance to the observer. The quantity $\omega B(T)$ is the flux that would be observed for a hot spot with unit emissivity. The contribution to the flux from the model hot spot, F_V, is reduced by its emissivity according to Eq. 1.

$$F_v = \tfrac{1}{2}(E_S + E_P)\omega B(T) \qquad (1)$$

where the emissivity for the radiation polarized with its electric vector parallel to the surface is

$$E_P = 1 - [(\cos\theta - s)/(\cos\theta + s)]^2 \quad (2)$$

the emissivity for the orthogonal polarization is

$$E_S = 1 - [(n^2\cos\theta - s)/(n^2\cos\theta + s)]^2 \quad (3)$$

and $s = (n^2 - \sin^2\theta)^{1/2}$. If this spot is viewed at a position angle ϕ, measured counterclockwise from north on Io, the component of the flux that is linearly polarized with its electric vector parallel to north is

$$F_x = \tfrac{1}{2}(E_S - E_P)\cos(2\phi)\omega B(T) \quad (4)$$

The flux component of the orthogonal linear polarization is

$$F_y = \tfrac{1}{2}(E_S - E_P)\sin(2\phi)\omega B(T) \quad (5)$$

If more than one hot spot is on the visible disk, then F_x, F_y, and F_v are the sum of the contributions from each spot. The total flux, F_t, is the background flux, F_b (*9*), plus the volcanic flux. A useful scaling for the total flux is an effective geometric albedo, p', that includes the volcanic component of the flux and is related to the true geometric albedo, p (*10*), by $p' = p(1 + F_v/F_b)$. The normalized Stokes' vector, $S = (1,x,y,z)$, is a complete description of the polarization state (*11*). In terms of the flux quantities defined above, x is F_x/F_t, y is F_y/F_t, and, because no circular polarization can be introduced at a dielectric boundary, z is 0. The degree of linear polarization, V, is $(x^2 + y^2)^{1/2}$, and the position angle of linear polarization, ψ, is 1/2 arctan (y/x).

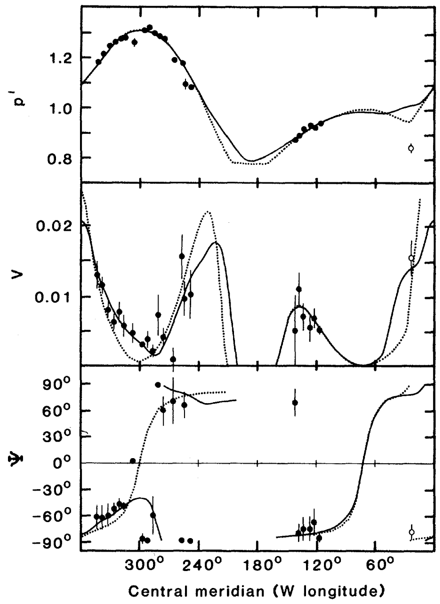

Fig. 2. Observations (●) and the best two-spot (. . . . . .) and three-spot models (———) of Io's 4.76 μm flux and linear polarization on 8, 9, and 10 July 1984 UT (Table 1). Observations on 13 August 1984 (○) were not included in the fit because of their nonsimultaneity with the other data. Error bars are ±1 standard deviation of the four to six independent measurements defining each point and indicate the internal consistency of the data. If $V = 0$, then ψ is undefined; ψ = +90° and −90° are equivalent.

As Io rotates both the solid angle and the directional emissivity of the spot vary, as does the disk-integrated linear polarization (Fig. 1). Polarization efficiency of the surface increases as the spot moves closer to the limb because of the strong angular dependence of the Fresnel coefficients. Simultaneously, the spot's contribution to the total flux decreases because of its rapidly decreasing apparent solid angle. These two trends combine to produce the characteristic pair of maxima in the degree of polarization. The plane of polarization is parallel to the line connecting the spot and the center of the disk. The central meridian longitude of the maximum flux, the minimum in the degree of polarization, and the zero crossing of the position angle all correspond to the longitude of the spot, and the asymptote of the position angle as the spot approaches the limb is the colatitude of the spot.

The flux and linear polarization of Io was measured at 4.76 μm effective wavelength (M filter) with an InSb detector and a rotating wire-grid polarimeter (*12*) at NASA's 3-m Infrared Telescope Facility on Mauna Kea, Hawaii (Fig. 2). Dates of observation were 8, 9, and 10 July 1984 universal time (UT), a period during which Io exhibited enhanced, but not unusual (*4*), 5-μm emission. These data (*13–15*) show that the polarization is variable with Io's rotation and that the degree of polarization is as large as 1.6 percent.

Simultaneous nonlinear least-squares fits for p', x, and y were made to determine the locations, relative sizes, and index of refraction of the emitting areas (*16*). Both systematic and statistical sources of error were evaluated (*17*) (Table 1). The data are naturally subdivided into two groups: extensive coverage on 8 and 10 July of the trailing hemisphere, and sparse coverage on 9 July of the leading hemisphere (*18*). Initial estimates of the parameters were obtained by fitting a one-spot model to the strong signature in the trailing hemisphere data (Figs. 1 and 2). Critical parameters not well known initially were the index of refraction and geometric albedo at 4.76-μm wavelength (*19*). Starting with n and p at their provisional one-spot values, the data from all three nights were fit to a two-spot model with the second spot lying on the leading hemisphere (Table 1). This two-spot model is the simplest one that reproduces the overall features of the observations.

Systematic deviations of the polarization data from the two-spot model between 300° and 360° west longitude and the large uncertainty in the latitude (compared to the longitude) of the spot on the trailing side indicate that a third spot might be present on the trailing hemisphere (Table 1 and Fig. 2). The best-fit solution including a third spot lying southwest of the larger, main spot is our preferred model. An alternate solution with somewhat larger residuals shifts the two spots to the northeast (Table 1) (*20*).

Locations and sizes of the hot spots on the trailing hemisphere (assuming a temperature of 450 K) (Table 1) were mapped relative to the major surface features discovered by Voyager (Fig. 3). The dominant source of 5-μm thermal emission is the region near Loki, which displayed two active plumes during the Voyager encounters and has been suggested as a stable, long-term source of 8.7- and 10-μm emission (*3*).

Our best position (288°W, 20°N) indicates that the source of the 5-μm emission is east and north of Loki Patera, a circular, low-albedo feature (200 km in diameter) that is thought to be a large

Table 1. Parameters of the least-squares best-fit models for two and three hot spots (T = 450 K) to observations of Io's disk-integrated linear polarization and flux. For each fit, the model parameters are shown together with the effects of systematic and statistical errors as the net change in the least significant digits. The sources of systematic error are the uncertainty in the zero point calibration of the M-magnitude flux scale and the M-magnitude of the sun, both of which affect the relative scaling of the flux and polarization data. The effects of these systematic errors are estimated by refitting the models for values of the M-magnitude of the sun ±0.06 magnitude about the optimum value. The effects of statistical measurement error are shown in parentheses below the parameter value as the value of 1 standard deviation, determined from 50 fits to an ensemble of 50 synthetic data sets generated with Gaussian noise comparable to that in the measurements (*17*). The value of χ^2 is the sum of the weighted squared residuals of p', x, and y. The combined effects of both sources of error are summarized together with the optimum parameter values. Alternate solutions for the three hot spots (bottom) represent a local minimum in χ^2, with parameter values and uncertainties that are not shown but are the same as those in the preferred three-spot solution.

Data	M (sun)	n	p	Hot spot 1			Hot spot 2			χ^2, hot spots 1 and 2	Hot spot 3			χ^2
				Area (km²)	Longitude (degrees)	Latitude (degrees)	Area (km²)	Longitude (degrees)	Latitude (degrees)		Area (km²)	Longitude (degrees)	Latitude (degrees)	
Two hot spots														
Systematic error (positive)	−6	−19	−63	−48	−9	+20	+83	+2.13	−70	+14				
Parameter	−28.23	1.467	0.784	4426	299.98	+8.80	1551	71.40	+5.61	628				
Standard error		(37)	(14)	(148)	(46)	(5.34)	(212)	(1.77)	(1.41)					
Systematic error (negative)	+6	+1	+48	+213	+1	0	+72	−9	+11	0				
Summary														
Total error (positive)		−6	−8	−200	+5	+6	+300	+4	−2					
Parameter		1.47	0.78	4430	300.0	+9	1550	71	+6					
Total error (negative)		+4	+6	+360	−5	−5	−140	−2	+2					
Three hot spots														
Systematic error (positive)	−6	−30	−56	−11	+28	−16	+45	+84	+22		−125	+1.78	−80	+6
Parameter	−28.23	1.507	0.788	3057	287.78	+20.08	1474	71.90	+6.44		1723	321.87	−11.62	492
Standard error		(45)	(14)	(118)	(2.70)	(1.34)	(212)	(3.30)	(1.43)		(116)	(5.52)	(4.28)	
Systematic error (negative)	+6	+17	+52	+50	−36	+32	+16	−18	−6		+143	−1.04	+72	+1
Summary														
Total error (positive)		−8	−7	−130	+3	−2	+260	+4	+2		−240	+7	−5	
Parameter		1.51	0.79	3060	288	+20	1470	72	+6		1720	322	−12	
Total error (negative)		+6	+7	+170	−3	+2	−200	−3	−1		+260	−7	+5	
Alternate for three hot spots														
Parameter					(311	−1)						277	+27	510

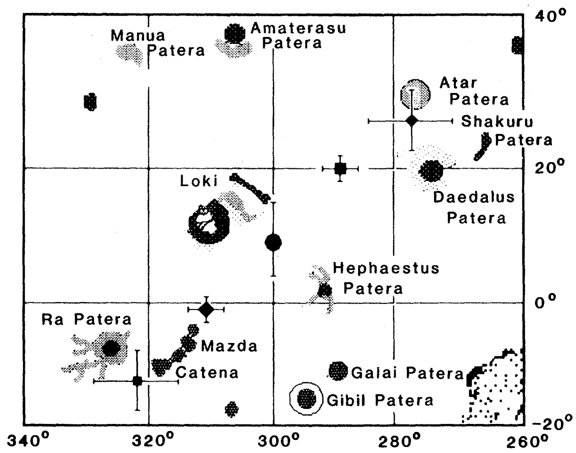

Fig. 3. Detailed map of the Loki region comparing the best two-spot fit (●) to the best three-spot fits (paired symbols ■ and ◆). The symbols are scaled to show the areas from Table 1. Note the northeast to southwest linear relation of the possible solutions.

lava lake. This location is consistent with the source lying near the east end of Loki, a linear, low-albedo feature (250 km in length) northeast of Loki Patera and the apparent source of plumes 2 and 9 seen by Voyager. This position suggests that the source may correspond to enhanced activity in the vicinity of plume 9, which grew considerably during the interval between Voyager encounters (*2*). The 3060-km^2 area corresponds to a circular hot spot 62 km in diameter, which is twice as large (in terms of flux emitted) as either of the remaining two spots but less than 10 percent of the low-albedo area of Loki Patera.

The position of the spot on the leading hemisphere (72°W, 6°N) corresponds to no named feature in the Voyager images. Voyager coverage was limited to low spatial resolution, and no IR spectroscopy was performed on this hemisphere. One possibility is that this feature represents an eruption that occurred after the Voyager encounters. The appearance of Surt and changes in Loki Patera between the two Voyager encounters attest to the volatile nature of Io's landscape (*1*). Another possibility is that the assumption of a single spot on the leading hemisphere is unjustified. The 1470-km^2 area of this spot corresponds to a circular region 43 km in diameter.

The preferred position for the third spot (322°W, 12°S) is nearest Ra Patera, a volcano that resembles some of the actively erupting features but was apparently dormant during the Voyager encounters. The error bars also encompass Mazda Catena (Fig. 3). The alternate position is close to Atar, a feature that is apparently the source of low-viscosity flows recently proposed as an example of sulfur volcanism (*21*). A circle 47 km in diameter has the same area, 1720 km^2, as the best-fit area for this spot.

In addition to determining the locations of the hot spots, this analysis yields the index of refraction of the emitting surface and the mean geometric albedo of the disk at 4.76-μm wavelength. The value for n of 1.51 (+0.06/−0.08) is close to that for some terrestrial basalts and basaltic glasses [1.34 to 1.46 (*22*)] and is lower than a measured value for sulfur [1.82 ± 0.07 at T = 35°C (*23*)]. Because macroscopic surface roughness will reduce the degree of polarization, the value for n of 1.51 should be regarded as a lower limit on the true index of refraction (*24*). The value for the mean geometric albedo, 0.79 ± 0.07, agrees well with measured values from 3.0 to 3.4 μm (*25*), which is the region of continuum toward shorter wavelengths from the SO_2 absorption band centered near 4 μm. It also agrees with the fraction of the total flux supplied by hot spots, measured by speckle interferometry during 2 to 4 July 1985 UT (*7*).

References and Notes

1. L. Morabito, S. P. Synnott, P. N. Kupferman, S. A. Collins, *Science* **204**, 972 (1979); G. G. Schaber, in *Satellites of Jupiter*, D. Morrison, Ed. (Univ. of Arizona Press, Tucson, 1982), pp. 556–597; T. V. Johnson and L. A. Soderblom, *ibid.*, pp. 634–646.
2. R. G. Strom and N. M. Schneider, in *Satellites of Jupiter*, D. Morrison, Ed. (Univ. of Arizona Press, Tucson, 1982), pp. 598–633.
3. T. V. Johnson *et al.*, *Science* **226**, 134 (1984); W. M. Sinton *et al.*, *ibid.* **210**, 1015 (1980).
4. W. M. Sinton *et al.*, *Icarus* **54**, 133 (1983); F. C. Witteborn, J. D. Bregman, J. B. Pollack, *Science* **203**, 643 (1979); J. C. Pearl and W. M. Sinton, in *Satellites of Jupiter*, D. Morrison, Ed. (Univ. of Arizona Press, Tucson, 1982), pp. 724–755.
5. C. E. Heiles and F. D. Drake, *Icarus* **2**, 281 (1963); R. Landau, *ibid.* **26**, 243 (1975); J. D. Jackson, *Classical Electrodynamics* (Wiley, New York, 1962), p. 216; K. J. Buettner and C. D. Kern, *J. Geophys. Res.* **70**, 1329 (1965).
6. P. E. Johnson *et al.*, *Icarus* **56**, 381 (1983).
7. Speckle interferometry by R. R. Howell and M. T. McGinn [*Science* **230**, 63 (1985)], made a few days preceding, and at the same wavelength as the observations reported here, successfully resolves Io's disk into a small number of elements.
8. J. Veverka, in *Planetary Satellites*, J. A. Burns, Ed. (Univ. of Arizona Press, Tucson, 1977), pp. 210–231. The phase angle was 2° at the time of observation and the degree of linear polarization was about −0.1 percent at 0.5 μm. The magnitude of the degree of polarization may be expected to be larger at longer wavelengths, but the high geometric albedo at 5 μm suggests that the polarization of reflected sunlight will also be small at 5 μm.
9. At 4.76 μm, the background flux is dominated by reflected sunlight and $F_b = (R/d)^2 p\pi F$, where R is Io's 1815-km radius and πF is the incident solar flux at Io's distance from the sun.
10. The geometric albedo is a dimensionless quantity that is the ratio of the flux measured to the flux that would be measured if Io were replaced by a perfectly diffusing disk of equal radius illuminated and viewed normally. A perfectly diffusing disk is one that obeys Lambert's law, which in the notation of (*9*) means that the intensity scattered by the disk is F.
11. W. A. Shurcliff, *Polarized Light* (Harvard Univ. Press, Cambridge, Mass., 1962); S. Chandrasekhar, *Radiative Transfer* (Dover, New York, 1960); K. Serkowski, *Adv. Astron. Astrophys.* **1**, 289 (1962).
12. H. M. Dyck and R. W. Capps, *Astrophys. J.* **220**, L49 (1978); H. M. Dyck and T. J. Jones, *Astron. J.* **83**, 594 (1978).
13. The x and y components of the instrumental polarization, as determined by the mean of each set of consecutive polarization sequences on the standard star (*14*), were linearly interpolated to the time of each Io sequence and subtracted from the observed x and y components of Io. On each night the scale for the analyzer position angle was calibrated by observing CRL 2591 (*15*). The flux for each sequence was the mean of the flux for the eight analyzer positions. An extinction coefficient was fit to the variation of the standard star flux with air mass, and the relative magnitude of Io to the standard, corrected for extinction, was determined. Primary M standards from the list of W. M. Sinton and W. C. Tittemore [*Astron J.* **89**, 1366 (1984)] were also observed to calibrate the M magnitude of λ Sgr, which was found to be 0.438 ± 0.005. The effective geometric albedo was calculated from Io's magnitude, its known radius and distance from Earth and the sun, and the magnitude of the sun (Table 1).
14. Our unpolarized standard was λ Sgr (Yale BS 6913), about 3° south of Jupiter on these dates. Typically, four to six independent polarization sequences, each consisting of eight analyzer positions with the signal integrated for 5 seconds at each position, were sandwiched between two pairs of standard star sequences. After each sequence, a peak algorithm was used to recenter the object.
15. S. G. Kleinmann and M. J. Lebofsky, *Astrophys. J.* **201**, L91 (1975); H. M. Dyck and C. J. Lonsdale, *Astron. J.* **85**, 1077 (1980). γ Cyg (Yale BS 7796) was used as a local unpolarized standard for CRL 2591. Our measured degree of polarization for CRL 2591 was 0.037, which is in excellent agreement with reported results. The position angle was calibrated to agree with the reported position angle for CRL 2591.
16. All fits used the simplex algorithm from M. S. Caceci and W. P. Cacheris [*Byte* **9**, 340 (1984)]. All points were weighted as $1/\sigma^2$, where σ is the standard deviation of the mean in each of the sets of x, y, and p' defining the point. In Eqs. 1, 4, and 5 the area and temperature occur only in the product $\omega B(T)$ and cannot be determined simultaneously unless polarization at more than one wavelength is measured. Temperature was fixed at 450 K. For other temperatures, the area of the hot spot will vary according to $A'/A = B(450\ \text{K})/B(T')$, where A is the area corresponding to 450 K (Table 1) and A' is the area corresponding to the temperature T'. Values of A'/A are 29, 2.3, 0.51, and 0.19 for values of T' of 300, 400, 500, and 600 K, respectively.
17. The principal source of statistical error was photon fluctuations of the background flux. The derived quantities p', x, and y are expected to preserve the Gaussian distribution of noise, but this preservation does not apply to V and ψ. The effects of statistical error on the parameters were evaluated from separate fits to each member of an ensemble of synthetic data sets. The ensemble comprised 50 synthetic data sets, with standard deviations of 0.01 in p' and of 0.001 in x and y, estimated from the reproducibility of the measurements (Table 1). The systematic error of ±0.06 magnitude in the flux scale is estimated from addition in quadrature of ±0.05 magnitude uncertainty in the zero point of the M-magnitude scale (H. C. Campins, G. H. Rieke, M. J. Lebofsky, Steward Observatory Preprint, 1985) and from ±0.02 magnitude uncertainty in the solar flux [J. E. Vernazza, E. H. Avrett, R. Loeser, *Astrophys. J. Suppl. Ser.* **30**, 1 (1976)].
18. The leading hemisphere is centered at 90°W and the trailing hemisphere at 270°W. This terminology refers to the hemisphere centered on the direction parallel (leading) or antiparallel (trailing) to the orbital velocity vector of a synchronously rotating satellite.
19. Our initial guess for n was 1.5 (a round number representative of some common terrestrial minerals) and for p was 0.85 on the basis of speckle

interferometry (7) that showed that the trailing-side point source contributed 30 to 40 percent of the total flux.
20. Performing an *F* test on the reduction of χ^2 obtained by the addition of the third hot spot and its additional three parameters shows that it is unlikely ($P < 0.01$) that a similar reduction of χ^2 would result from a fortuitous distribution of data.
21. R. Greeley and J. H. Fink, *Astron. Express* **1**, 25 (1984).
22. J. B. Pollack, O. B. Toon, B. N. Khare, *Icarus* **19**, 372 (1973).
23. W. M. Sinton, unpublished results from measurements of interference fringes produced by a known thickness of recrystallized S_8 at 308 K sandwiched between two Si plates. Direct measurements of the index of refraction of molten sulfur at 2 μm and 450 K [E. T. Arakawa *et al.*, *Bull. Astron. Astrophys. Soc.* **16**, 653 (1984)] indicate that $n = 1.84$ and that it decreases slowly with wavelength.
24. Our model assumes that the emitting surface is flat and smooth on the wavelength scale. This is justifiable if we are seeing the surface of a quiescent, molten lava lake but is less so if we are seeing cooling flows with textures resembling Hawaiian aa. In general, a rough surface will exhibit less polarization than a similar smooth one because the average viewing angle is reduced for a rough surface by the preference for the observer to see slopes whose normal is in the direction of the line of sight and for the disappearance of slopes slanted in the opposite direction.
25. R. R. Howell, D. P. Cruikshank, F. P. Fanale, *Icarus* **57**, 83 (1984). Variation of *p* with longitude is not considered in this analysis and is assumed to be negligible on the basis of the small variation measured in the continuum from 3.0 to 3.4 μm.
26. The authors are visiting astronomers at the Infrared Telescope Facility (IRTF), operated by the University of Hawaii under contract from the National Aeronautics and Space Administration. Supported in part by NASA grant NGL 12-001-057 and NSF grant AST83-11105. We thank R. R. Howell for providing data in advance of publication; the IRTF staff, particularly R. Capps, R. Koehler, and C. Kaminski, for assistance; and R. R. Howell and H. M. Dyck for helpful discussions.

12 March 1985; accepted 26 July 1985

Nodal Modulation of the Lunar Semidiurnal Tide in the Bay of Fundy and Gulf of Maine

Abstract. *Observations, numerical modeling, and theoretical calculations show how the 18.6-year modulation of the main lunar semidiurnal tide in the Bay of Fundy and Gulf of Maine is reduced from its astronomical value of 3.7 percent to 2.4 percent by the effects of friction and resonance. The agreement of the three approaches increases confidence in model predictions of widespread changes in the tidal regime resulting from development of tidal power.*

L.-F. Ku
Fisheries and Oceans Canada,
Canadian Hydrographic Service,
Ottawa, Ontario K1A 0E6
D. A. Greenberg
Fisheries and Oceans Canada,
Coastal Oceanography,
Bedford Institute of Oceanography,
Dartmouth, Nova Scotia B2Y 4A2
C. J. R. Garrett
Department of Oceanography,
Dalhousie University,
Halifax, Nova Scotia B3H 4J1
F. W. Dobson
Fisheries and Oceans Canada,
Ocean Circulation,
Bedford Institute of Oceanography

The world's highest tides occur in the Bay of Fundy and have been attributed (*1*) to a near-resonant response of the Bay of Fundy–Gulf of Maine system. Proposed development of tidal power would increase the tides throughout this region by bringing the system closer to resonance. Detailed predictions of this increase have been made by a numerical model (*2*) that has been calibrated against observed tides. We report that study of the long-period variations in the tide support the idea of resonance and the validity of the numerical model.

The astronomical forcing of the main lunar semidiurnal tide (M_2 tide), which has a period of 12.42 hours, varies by ±3.73 percent during 18.61 years because of variations in the declination of the moon's orbit (*3*). It is generally assumed in tidal prediction that the observed M_2 tide will be modulated by the same amount. In the few instances in which long records of sea level have been analyzed to check this assumption (*4, 5*), they show noticeable differences from the astronomical values. Using more recent data, we examined the departure of the modulation of M_2 from the value predicted in the equilibrium tide and we compared our results with those from a numerical model and from theoretical calculations.

An unmodulated tidal constituent would take the form of $A\cos(\omega t - \theta)$, where A is amplitude, ω is the tidal frequency, t is time, and θ is a phase lag. The theoretically modulated tide may be written $A(1 + R\cos\Delta t)\cos(\omega t - \theta + u)$ where $\Delta = -2\pi(18.61\ \text{years})^{-1}$, $u = -R\sin\Delta t$. As mentioned, for the M_2 tide, $R = 0.0373$ and so $|u|$ is 2.14°. Because the observed tide may be different from this, we consider it in the form $A[1 + R'\cos(\Delta t - \delta')]\cos(\omega t - \theta + u')$, where $u' = -a\sin\Delta t + b\cos\Delta t$, with R', δ', a, and b to be determined from the data. When the observed modulation equals the theoretical astronomical modulation, $R' = R$, $\delta' = 0$, $a = R$, and $b = 0$.

Data on sea level from Saint John (Fig. 1) for the years 1947 through 1971 were Fourier analyzed at the M_2 frequency for each year and the amplitude and phase fitted with our model. The results may be compared (Table 1) with those of a similar analysis by Doodson (*4*) for 1894 through 1916. Data from Boston and Bar Harbor for 1947 through 1966 were analyzed by complex demodulation. To ensure that we were looking at the response of the Fundy-Maine system and not the North Atlantic, data from Halifax for 1920 to 1980 were also analyzed.

The numerical model of Greenberg (*2*) was used with the imposed M_2 tide at the shelf edge increased by 3.73 percent ($R = 0.0373$) to see how well the model response corresponded to observation. To account for open boundaries (*6*), a trial was also made with boundary amplitudes scaled up by 4.0 percent.

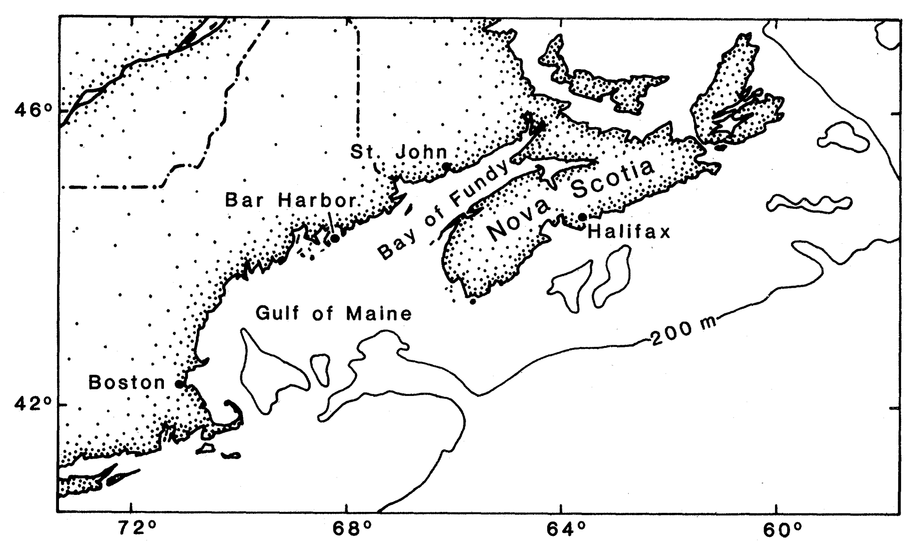

Fig. 1. The Bay of Fundy and Gulf of Maine.